

Editor's Pick | Antimicrobial Chemotherapy | Full-Length Text

# Development of non-sedating benzodiazepines with *in vivo* antischistosomal activity

Md Yeunus Mian,<sup>1,2</sup> Dishary Sharmin,<sup>1,2</sup> Prithu Mondal,<sup>1,2</sup> Jawad Bin Belayet,<sup>1,2</sup> M. Mahmun Hossain,<sup>1,2</sup> Paul McCusker,<sup>3</sup> Kaelyn T. Ryan,<sup>4</sup> Alexander Y. Fedorov,<sup>5</sup> Heather A. Green,<sup>5</sup> Spencer S. Erickson,<sup>5</sup> Mostafa Zamaniyan,<sup>4</sup> V. V. N. Phani Babu Tiruveedhula,<sup>1</sup> James M. Cook,<sup>1,2</sup> John D. Chan<sup>3,4,6</sup>

**AUTHOR AFFILIATIONS** See affiliation list on p. 16.

**ABSTRACT** The neglected tropical disease schistosomiasis infects over 200 million people worldwide and is treated with just one broad-spectrum antiparasitic drug (praziquantel). Alternative drugs are needed in the event of emerging praziquantel resistance or treatment failure. One promising lead that has shown efficacy in animal models and a human clinical trial is the benzodiazepine meclonazepam, discovered by Roche in the 1970s. Meclonazepam was not brought to market because of dose-limiting sedative side effects. However, the human target of meclonazepam that causes sedation ( $\text{GABA}_{\text{A}}\text{Rs}$ ) is not orthologous to the parasite targets that cause worm death. Therefore, we were interested in whether the structure of meclonazepam could be modified to produce antiparasitic benzodiazepines that do not cause host sedation. We synthesized 18 meclonazepam derivatives with modifications at different positions on the benzodiazepine ring system and tested them for *in vitro* antiparasitic activity. This identified five compounds that progressed to *in vivo* screening in a murine model, two of which cured parasite infections with comparable potency to meclonazepam. When these two compounds were administered to mice that were run on the rotarod test, both were less sedating than meclonazepam. These findings demonstrate the proof of concept that meclonazepam analogs can be designed with an improved therapeutic index and point to the C3 position of the benzodiazepine ring system as a logical site for further structure–activity exploration to further optimize this chemical series.

**KEYWORDS** schistosomiasis, anthelmintic, benzodiazepine

While the neglected tropical disease schistosomiasis infects over 200 million people worldwide (1), control of the disease is almost entirely reliant on one drug, praziquantel (PZQ). A recent meta-analysis of PZQ efficacy over four decades indicates cure rates between 57% and 88% (2), but there is the concern that resistance may emerge with repeated rounds of mass drug administration (3). Parasite resistance can be selected in the laboratory (4–6), and there are numerous reports of treatment failure in the field (7, 8). An alternative antischistosomal drug would be of obvious use in the event of either PZQ treatment failure or resistance. However, older antischistosomal chemotherapies tend to either have unacceptable toxicity (e.g., antimony compounds) or lack broad efficacy against the two species of schistosomes infecting humans in Africa [e.g., oxamniquine is only effective against *Schistosoma mansoni* (9), and metrifonate is only effective against *Schistosoma haematobium* (10)]. Benzodiazepines are promising antischistosomal candidates because they are effective against both of these African species (11, 12). Binding and functional assays indicate that meclonazepam (MCLZ) and PZQ do not appear to act on the same target (13, 14). Additionally, unlike PZQ, MCLZ can cure schistosomiasis at the juvenile, liver stage of parasite infections (11, 15).

**Editor** Audrey Odom John, The Children's Hospital of Philadelphia, Philadelphia, Pennsylvania, USA

Address correspondence to John D. Chan, jchan32@wisc.edu.

The authors declare no conflict of interest.

See the funding table on p. 17.

**Received** 7 March 2024

**Accepted** 9 July 2024

**Published** 13 August 2024

Copyright © 2024 American Society for Microbiology. All Rights Reserved.

The antischistosomal activity of MCLZ (also referred to as Ro 11-3128 or 3-methyl clonazepam) was discovered by Roche in the late 1970s in a screen of over 400 benzodiazepines (11). The drug was advanced to a small human trial and found to cure infections with *S. mansoni* and *S. haematobium* (12). However, patients also experienced pronounced sedative side effects at doses required for antischistosomal activity. Attempts were made to block this sedation—the GABA<sub>A</sub>R antagonist flumazenil was developed and was shown to have no impact on the antiparasitic effect of MCLZ (16). However, flumazenil only transiently antagonized MCLZ sedation when the two drugs were given together (17) due to pharmacokinetic differences between the two drugs [flumazenil has a half-life of less than 1 hour (18), while MCLZ's half-life can be up to 40 hours (19)].

While MCLZ and other benzodiazepines cause sedation due to positive allosteric modulator (PAM) activity at human GABA<sub>A</sub>R chloride channels, these compounds exert antiparasitic effects through different schistosome targets. The sequenced genomes of parasitic flatworms lack GABA<sub>A</sub>Rs (20–22), indicating that it is unlikely the parasite targets of benzodiazepines such as MCLZ are homologous to the human GABA<sub>A</sub>Rs receptors that cause sedation (23). The initial studies on MCLZ's effects on schistosomes in the 1970s showed that the drug causes rapid Ca<sup>2+</sup> influx, muscle contraction, and tegument damage (24). MCLZ was recently shown to act as an agonist at a Ca<sup>2+</sup>-permeable schistosome transient receptor potential (TRP) channel (14), identifying the likely parasite receptor for this drug. This finding that MCLZ acts on a TRP channel is consistent with the original Roche screening data that the vast majority of benzodiazepines which are known potent agonists or PAMs of mammalian GABA<sub>A</sub>Rs do not have antischistosomal activity (11, 13, 21). Because the host and parasite targets are different, we reasoned it should be feasible to develop MCLZ derivatives that retain antischistosomal activity but exhibit reduced sedation. Past work from our labs supported this hypothesis. We found that benzodiazepines known to lack α1GABA<sub>A</sub>R affinity exhibit *in vitro* antischistosomal activity (21), which led us to expand our screen to further explore the structure–activity relationship of these compounds on parasites.

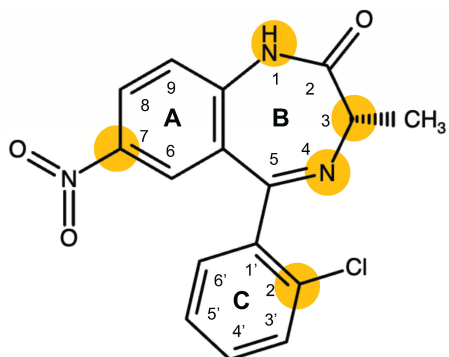
Here, we have screened 18 new compounds with a focus on molecules with modifications near the C3 position of MCLZ, which could be tolerated without loss of antiparasitic activity. Two compounds were confirmed to exhibit *in vivo* efficacy against *S. mansoni* while displaying a lack of sedation, or greatly reduced sedation, relative to the parent molecule MCLZ.

## RESULTS

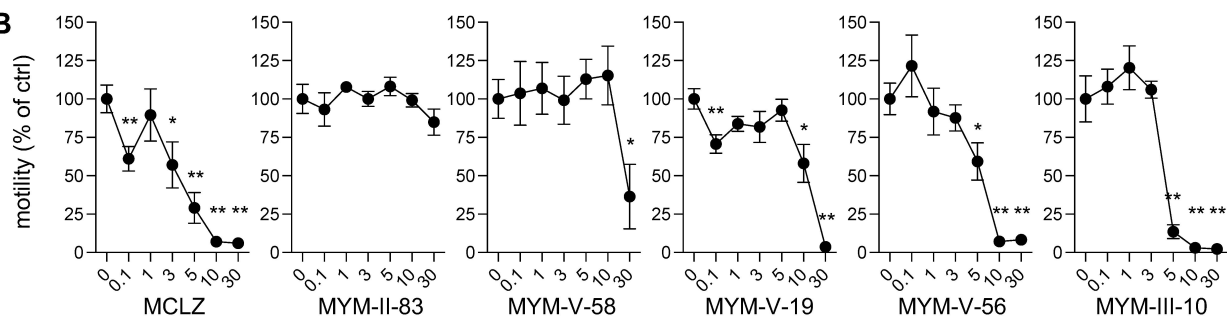
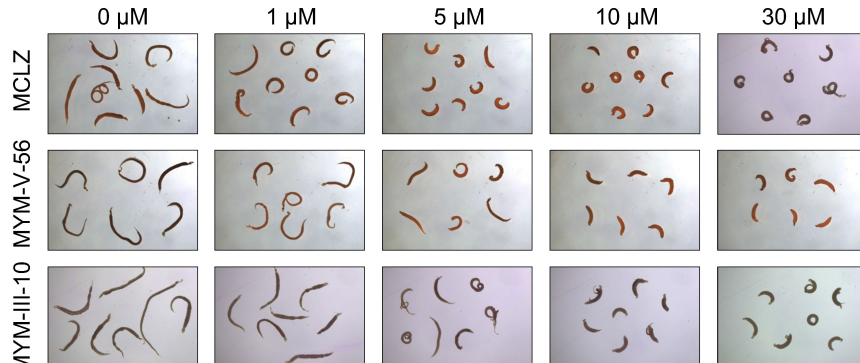
### *In vitro* screen of MCLZ derivatives on adult schistosomes

In order to identify antiparasitic benzodiazepines with decreased sedative potential, we synthesized MCLZ derivatives with modifications at various positions and first determined whether they retained antischistosomal activity. We synthesized 18 derivatives with modifications to the N1, C3, N4, C7, and C2' positions of the benzodiazepine ring system (Fig. 1A; Table S1) and screened these compounds at a high concentration (30 μM for 14 hours) against adult *S. mansoni* *in vitro* to triage inactive compounds. Active compounds caused worm contractile paralysis, while worms incubated with inactive compounds remained motile with no visible change in worm movement or morphology (Fig. 1A). Many positions on MCLZ were not amenable to substitution. Analogs with modifications at the N1 (MYM-II-53), N4 (MYM-V-48 and MYM-V-49), and C7 (MYM-V-03, MYM-IV-01, MYM-IV-02, MYM-IV-03, MYM-IV-12, MYM-IV-63, and MYM-II-72) lacked activity in this initial assay. However, modification of the C3 position was more variable. While some compounds were inactive (MYM-II-53, MYM-II-74, and MYM-V-50), other modifications did retain activity (MYM-V-19, MYM-II-83, MYM-V-56, MYM-III-10, and MYM-V-58).

Compounds that exhibited antischistosomal activity in this initial screen were then assayed at a series of decreasing concentrations to explore their structure–activity relationship. Adult *S. mansoni* were incubated in compound (0.1–30 μM for 14 hours), and motility was measured using a high content imaging system and the wrmXpress

**A**

Compound	1	3	4	7	2'	Phenotype
MCLZ	H	CH <sub>3</sub>	N	NO <sub>2</sub>	Cl	Paralysis
MYM-II-53	CH <sub>3</sub>	CH <sub>3</sub>	N	NO <sub>2</sub>	Cl	Motile
MYM-II-74	H	CH <sub>3</sub> , CH <sub>3</sub>	N	NO <sub>2</sub>	Cl	Motile
MYM-V-51	H	OCH <sub>3</sub>	N	NO <sub>2</sub>	Cl	Motile
MYM-II-83	H	CH <sub>3</sub> COO	N	NO <sub>2</sub>	Cl	Paralysis
MYM-III-10	H	OH	N	NO <sub>2</sub>	Cl	Paralysis
MYM-V-19	H	CH <sub>2</sub> CH <sub>3</sub>	N	NO <sub>2</sub>	Cl	Paralysis
MYM-V-50	H	O	N	NO <sub>2</sub>	Cl	Motile
MYM-V-56	H	F	N	NO <sub>2</sub>	Cl	Paralysis
MYM-V-48	H	6 membered ring, C-pyridine		NO <sub>2</sub>	Cl	Motile
MYM-V-49	H	6 membered ring, C-NH <sub>2</sub>		NO <sub>2</sub>	Cl	Motile
MYM-V-58	H	OH	N	NO <sub>2</sub>	F	Paralysis
MYM-V-03	H	CH <sub>3</sub>	N	H	Cl	Motile
MYM-IV-01	H	CH <sub>3</sub>	N	C <sub>6</sub> H <sub>5</sub> CN	Cl	Motile
MYM-IV-02	H	CH <sub>3</sub>	N	C <sub>6</sub> H <sub>5</sub> CF <sub>3</sub>	Cl	Motile
MYM-IV-03	H	CH <sub>3</sub>	N	C <sub>6</sub> H <sub>5</sub> OCH <sub>3</sub>	Cl	Motile
MYM-IV-12	H	CH <sub>3</sub>	N	CN	Cl	Motile
MYM-IV-63	H	CH <sub>3</sub>	N	C <sub>3</sub> H <sub>6</sub>	Cl	Motile
MYM-II-72	H	CH <sub>3</sub>	N	C <sub>2</sub> H <sub>2</sub> C(CH <sub>3</sub> ) <sub>3</sub>	F	Motile

**B****C**

**FIG 1** *In vitro* effects of MCLZ analogs on adult *S. mansoni*. (A) Top: structure of MCLZ with the benzodiazepine ring system numbered and the modified positions highlighted in yellow. Bottom: MCLZ analogs synthesized with modifications to various positions (1, 3, 4, 7, and 2') on the benzodiazepine ring system. Adult *S. mansoni* (five to 10 worm pairs) were incubated with compound *in vitro* (30 μM for 14 hours), and the resulting phenotype is noted (paralysis). (Continued on next page)

**FIG 1 (Continued)**

indicating active compounds and motile indicating compounds with no noticeable effects on movement/morphology). (B) Concentration–response curves showing potency of compounds shown to be active in A. Motility is normalized to movement of DMSO control-treated worms (values reflect mean  $\pm$  standard error of  $n = 8$  worms), and significance of differences between drug cohorts and DMSO control is reflected by \* $P < 0.05$  and \*\* $P < 0.01$  (unpaired t-tests). (C) Comparison of the morphology of worms treated with MCLZ and the two most potent compounds, MYM-V-56 and MYM-III-10.

pipeline to quantify worm movement (25, 26). Most of these compounds were less active than MCLZ, but two compounds (MYM-V-56 and MYM-III-10) with substitutions at the C3 position retained antischistosomal activity at potency near the parent molecule MCLZ (Fig. 1B and C). The effects of these compounds on motility (Fig. 1B) and morphology (Fig. 1C) were observed to be slightly less potent than MCLZ. However, MYM-V-56 and MYM-III-10 were initially screened as racemic mixtures, while MCLZ is the purified (S) enantiomer of 3-methyl clonazepam, and the (R) enantiomer has been reported to be inactive on parasites (27).

#### ***In vivo* efficacy of benzodiazepine leads in a murine model of schistosomiasis**

In order to determine whether hit compounds identified as having *in vitro* activity at 30  $\mu$ M displayed *in vivo* antischistosomal activity, they were administered to mice infected with *S. mansoni*, and the hepatic shift assay was used to observe acute antischistosomal activity, similar to the original Roche study on MCLZ (11). Adult worms normally live within the mesenteric vasculature, but upon exposure to anthelmintic compounds, paralyzed worms are swept through the portal vein to the liver (28). Mice were administered compound by oral gavage at a dose of 100 mg/kg and then euthanized 3 hours later to observe the portion of worms in the liver versus the mesenteries (Fig. 2A). Following MCLZ treatment, 100% of worms were found in the liver, and no worms were found in the mesenteries of any mice. Following treatment with the two compounds that showed greatest *in vitro* efficacy, MYM-V-56 and MYM-III-10, 100% of worms were located in the liver, and no worms were found in the mesenteries. Generally, compounds that showed weaker potency *in vitro* were less active in the hepatic shift assay. MYM-V-19 was only active at the highest concentration (30  $\mu$ M) *in vitro* and caused little hepatic shift ( $5.0 \pm 3.2\%$  of worms were found in the liver). MYM-V-58 was similarly only weakly active *in vitro* but caused a moderate hepatic shift ( $60.0 \pm 23.4\%$  of worms were found in the liver). MYM-II-83, which contains an ester at the C3 position that is likely hydrolyzed *in vivo*, was not active *in vitro* but displayed moderate activity *in vivo* ( $81.0 \pm 10.6\%$  hepatic shift). When comparing drugs to each other, MYM-V-58 and MYM-II-83 show no statistically significant difference, and MYM-II-83 shows no significant difference to MYM-III-10 or MYM-V-56.

The three most efficacious compounds, MYM-III-10, MYM-V-56, and MYM-II-83, were then administered to mice (single oral dose of 100 mg/kg) and euthanized after 1 week to count the number of surviving worms. Mice treated with vehicle control harbored  $39.4 \pm 4.0$  worm pairs, but no live worms were found in MCLZ-, MYM-III-10-, or MYM-V-56-treated mice (Fig. 2B). Mice treated with MYM-II-83 did not have any reduction in worm burden compared to control ( $40.0 \pm 0.6$  worm pairs per mouse), in contrast to the moderate acute activity of this compound in the hepatic shift assay.

Given that MYM-V-56 and MYM-III-10 exhibited acute *in vivo* efficacy and cured infections at 100 mg/kg, we assessed the potency of these compounds relative to MCLZ by treating infected mice with a range of doses (10–90 or 120 mg/kg) and counting the live worm burden after 1 week (Fig. 2C). MCLZ cured infected mice at a dose of 30 mg/kg, in line with the effective dose between 33 and 57 mg/kg reported in the initial Roche study (11). MYM-V-56 and MYM-III-10 displayed curative activity at higher doses of 90–120 mg/kg. This is consistent with the *in vitro* results where the racemate of these compounds was slightly less potent than MCLZ, which is the purified active (S) isoform (Fig. 1B and C).

Finally, one of the unique features of MCLZ compared to other antischistosomal drugs such as PZQ or oxamniquine is that MCLZ is active against juvenile liver stages of

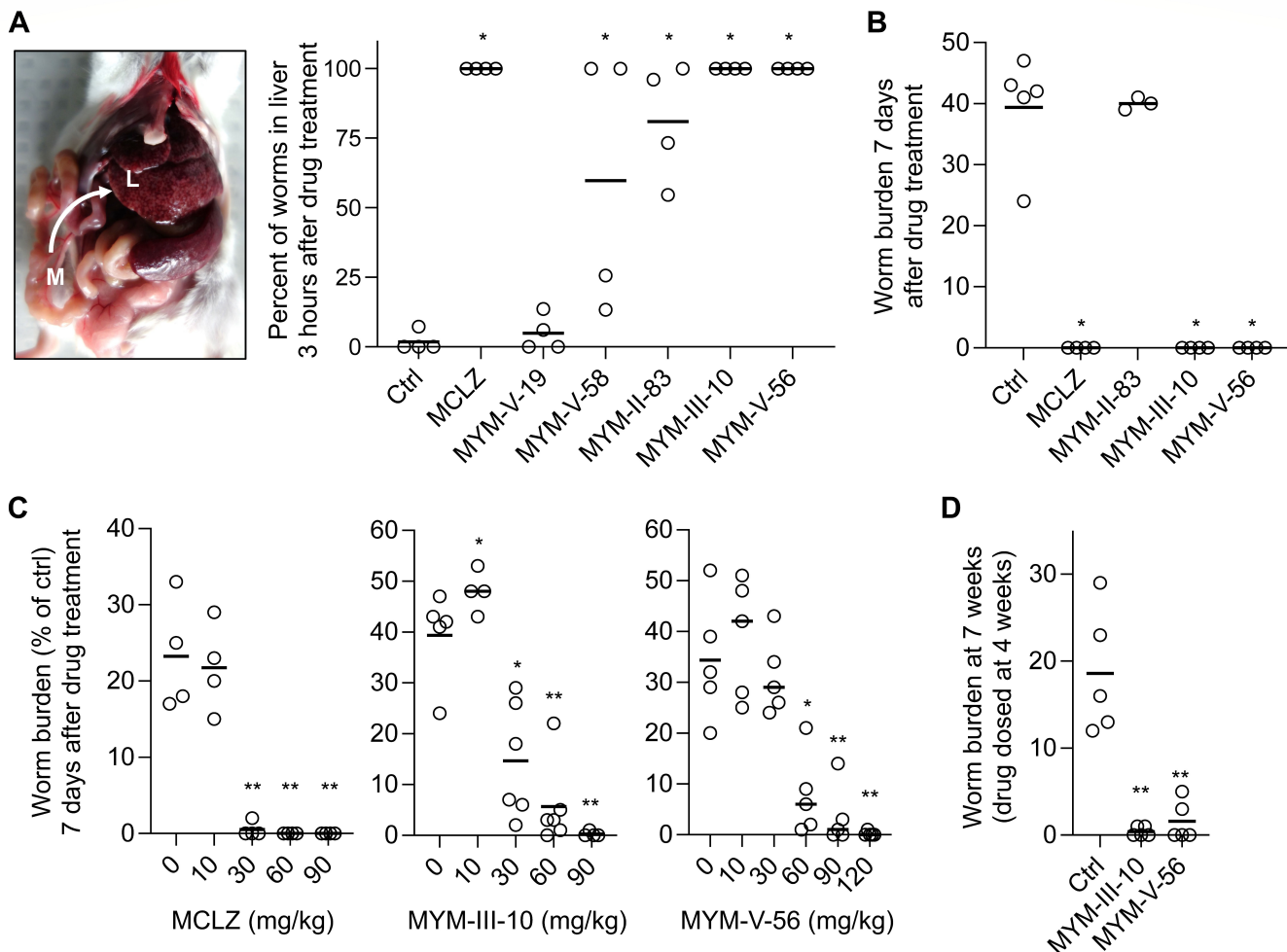


**FIG 2** *In vivo* effect of MCLZ analogs on *S. mansoni*. (A) Acute *in vivo* antischistosomal activity of MCLZ derivatives, assayed by measuring the percentage of worms in the liver as opposed to the mesenteric vasculature following drug treatment (oral dose of 100 mg/kg). Open symbols reflect percentages for individual mice ( $n = 4$  per condition); solid bars indicate the mean percentage for the treatment cohort. An image illustrating the relevant mouse anatomy and direction of the parasite hepatic shift from the mesenteric vasculature (M) to the liver (L) is shown, reproduced from reference (29). (B) Curative activity of MCLZ derivatives following a single oral dose of 100 mg/kg. Mice were euthanized 1 week after drug administration, and worm burden was measured. Bar = mean value, and open symbols reflect worm burdens for individual mice (between  $n = 3$ –5 mice per treatment condition). (C) Potency of MCLZ, MYM-III-10, and MYM-V-56 at curing infections of adult *S. mansoni*. Bar = mean value, and open symbols reflect worm burdens for individual mice (between  $n = 4$ –6 mice per treatment condition). (D) Curative activity of MYM-III-10 and MYM-V-56 against juvenile, liver stage parasites. Open symbols reflect the worm burden of individual mice ( $n = 5$  mice per condition); solid bars indicate the mean percentage for the treatment cohort. Significance of differences between drug treatments and DMSO control is reflected by \* $P < 0.05$  and \*\* $P < 0.01$  (Mann-Whitney *U* test).

worms (11, 30). Therefore, we wanted to confirm that MYM-V-56 and MYM-III-10 were also capable of clearing these stages of parasites. Infected mice were dosed with both compounds (100 mg/kg) at 4 weeks post-infection, which corresponds to the period where PZQ displays the least efficacy. Mice were then euthanized at 7 weeks post-infection to count the surviving worms. A single dose of either MYM-V-56 or MYM-III-10 reduced parasite burden by over 90% (Fig. 2D).

We conducted these initial experiments on MYM-III-10 and MYM-V-56 with racemic preparations of compound, given the resources involved in achieving enantiomeric separation of the (R) and (S) isomers at sufficient scale for *in vivo* mouse studies. However, we reasoned that the purified (S) enantiomers would be more potent, as is the case with (S)- versus (R)-MCLZ (27). The two enantiomers of MYM-III-10 and MYM-V-56 were separated by preparative high-performance liquid chromatography (HPLC), and adult

worms were incubated in each compound *in vitro* to observe paralysis. For MYM-V-56, both the (S) and (R) enantiomers caused contractile paralysis of worms above 5  $\mu\text{M}$  after

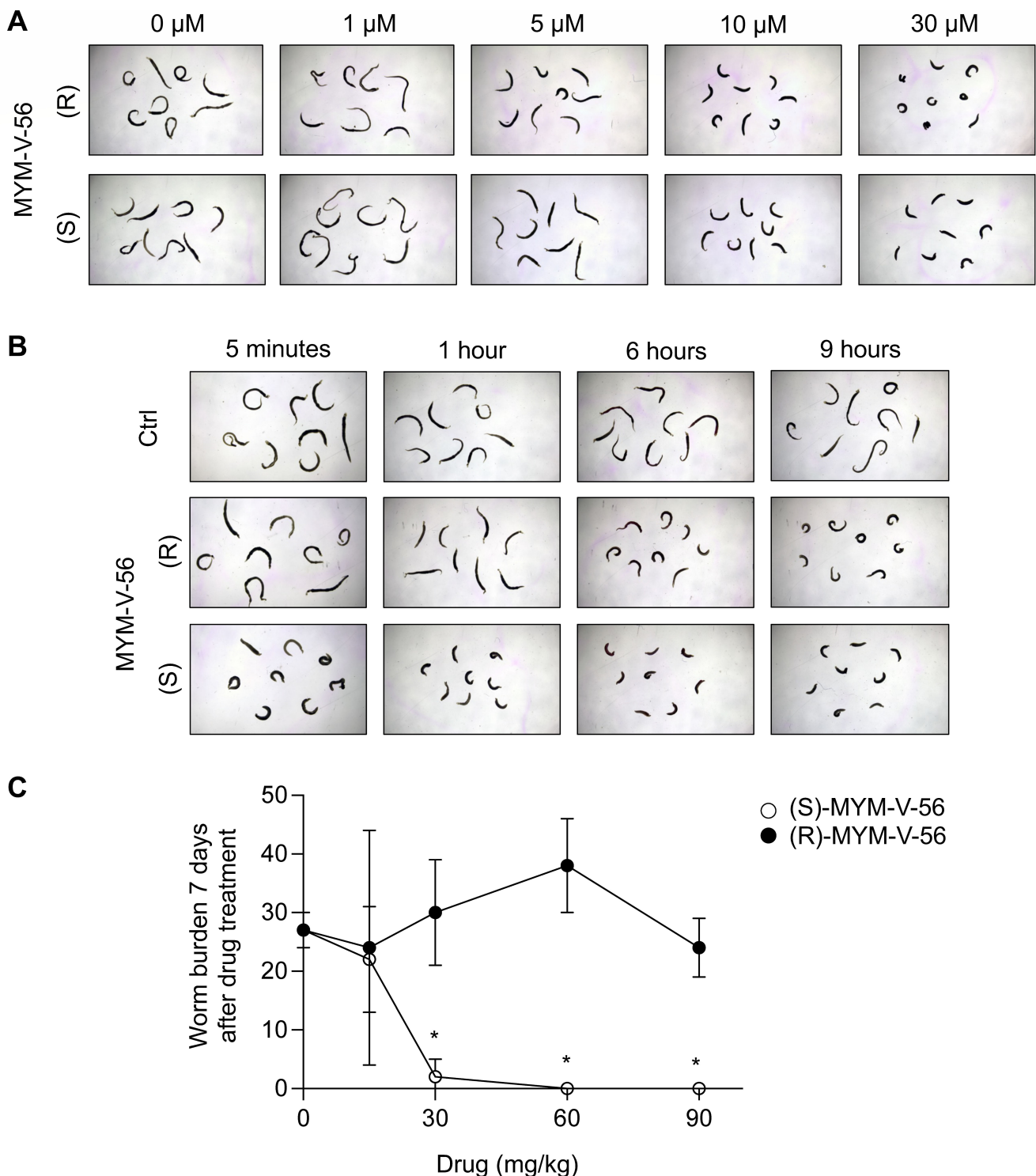


**FIG 3** Antischistosomal activity of MYM-V-56 enantiomers. (A) *In vitro* effect of purified (R)- and (S)-MYM-V-56 enantiomers on adult worms (14-hour incubation). (B) Time course of the onset of contractile paralysis caused by each enantiomer (10  $\mu\text{M}$  incubation for each). (C) *In vivo* efficacy of each MYM-V-56 enantiomer against adult parasites. Mice ( $n = 4$ –6 per drug treatment) were dosed with various amounts of each compound 6 weeks post-infection and euthanized 1 week later to assess worm burden. Symbols denote mean  $\pm$  standard error. Significance of differences between drug treatments and DMSO control is reflected by \* $P < 0.05$  (Mann-Whitney  $U$  test).

14 hours of incubation (Fig. 3A). While these two compounds initially appear equipotent from these data, the kinetics of drug action were quite different. Worms were incubated in 10  $\mu$ M of each enantiomer and tracked over time. (S)-MYM-V-56 caused contractile paralysis within minutes, while the (R) enantiomer did not cause this phenotype until after several hours of incubation in drug (Fig. 3B). It is likely that the (S) enantiomer is more active *in vivo*, because of the rapid kinetics of the hepatic shift observed with racemic MYM-V-56 treatment (Fig. 2A). This was confirmed by dosing mice harboring adult parasites orally with both enantiomers. Mice were euthanized 1 week after drug administration to assess worm burden and *in vivo* antischistosomal activity of each compound. (S)-MYM-V-56 caused a reduction in worm burden of more than 90% at 30 mg/kg ( $2 \pm 3$  worm pairs per mouse, compared to  $27 \pm 3$  worm pairs per mouse with vehicle control), while (R)-MYM-V-56 did not decrease worm burden up to the highest dose tested (90 mg/kg) (Fig. 3C).

Worms incubated with various concentrations of both (S)- and (R)-MYM-III-10 for 14 hours also displayed contractile paralysis, with the (S) enantiomer displaying greater potency than the (R) enantiomer (Fig. 4A). Unlike MYM-V-56, both enantiomers displayed *in vivo* activity, with (S)-MYM-III-10 curing infections at 60 mg/kg, while (R)-MYM-III-10 cured infections at 90 mg/kg (Fig. 4B). However, given the hydroxyl group on the C3 position of this compound, we anticipated that this compound may racemize over time in aqueous solution. This has been shown for other benzodiazepines with a C3 hydroxy substituent (e.g., oxazepam, lorazepam, and temazepam) (31). Indeed, purified MYM-III-10 enantiomers racemized within 1 hour (Supplemental File S1). Therefore, (S)-MYM-III-10 may still be more active than the (R) isoform, if much of the antischistosomal activity seen with the (R) enantiomer is in fact due to conversion to the (S) form.

### *In vivo* sedative activity of benzodiazepine lead compounds

Given that both MYM-V-56 and MYM-III-10 both retain the antischistosomal activity of MCLZ, we assessed the sedative activity of these compounds. Mice were trained to perform the rotarod test, running on the rod for 300 seconds at a speed of 20 RPM. Animals not infected with schistosomiasis were chosen for this assay, because the hepatomegaly caused by parasite infection can interfere with mouse mobility. Animals were dosed orally with increasing amounts of MCLZ or test compound and after 5 minutes were placed on the rotarod device to perform the test. Whenever a mouse fell off of the device, this time point was noted, and the test was ended for that animal. For all other animals, the test was ended at 300 seconds. Mice dosed with MCLZ displayed impaired performance on the rotarod test, consistent with this assay serving as a measurement of sedation. At the dose of 30 mg/kg (which corresponds to the dose that cures infection), only 2/14 mice were able to complete the test, and the average time they were able to run on the device was  $102 \pm 26$  seconds (Fig. 5). Mice treated with MYM-III-10 (30 mg/kg) exhibited less impairment, running on the device for an average of  $246 \pm 26$  seconds, and mice treated with MYM-V-56 (30 mg/kg) ran on the device for an average of  $232 \pm 30$  seconds. The purified (R)- and (S)-MYM-V-56 enantiomers were also tested and displayed minimal sedation, running for  $293 \pm 8$  seconds and  $299 \pm 1$  seconds, respectively, at 30 mg/kg dose.

While it may appear from these results that MYM-V-56 does not impair mouse locomotion/coordination, observing the mice in their cages following treatment indicates that this compound does have psychoactive effects, even if it is not sedating. Videos of mice treated with vehicle control, MCLZ, and MYM-V-56 (100 mg/kg each) are shown in Supplemental File S2 to S4. MYM-V-56-treated mice appear unusually hyperactive. In fact, in order to record a 20-second video of these mice, it was necessary to place a plexiglass cover over the cage to keep them from jumping out and escaping. Psychoactive effects are subtly seen at 30 mg/kg but are most apparent at doses 60 mg/kg and higher. We also observed mice treated with MYM-V-56 that did not complete the rotarod test did not appear sedated. Instead, they would jump off of the

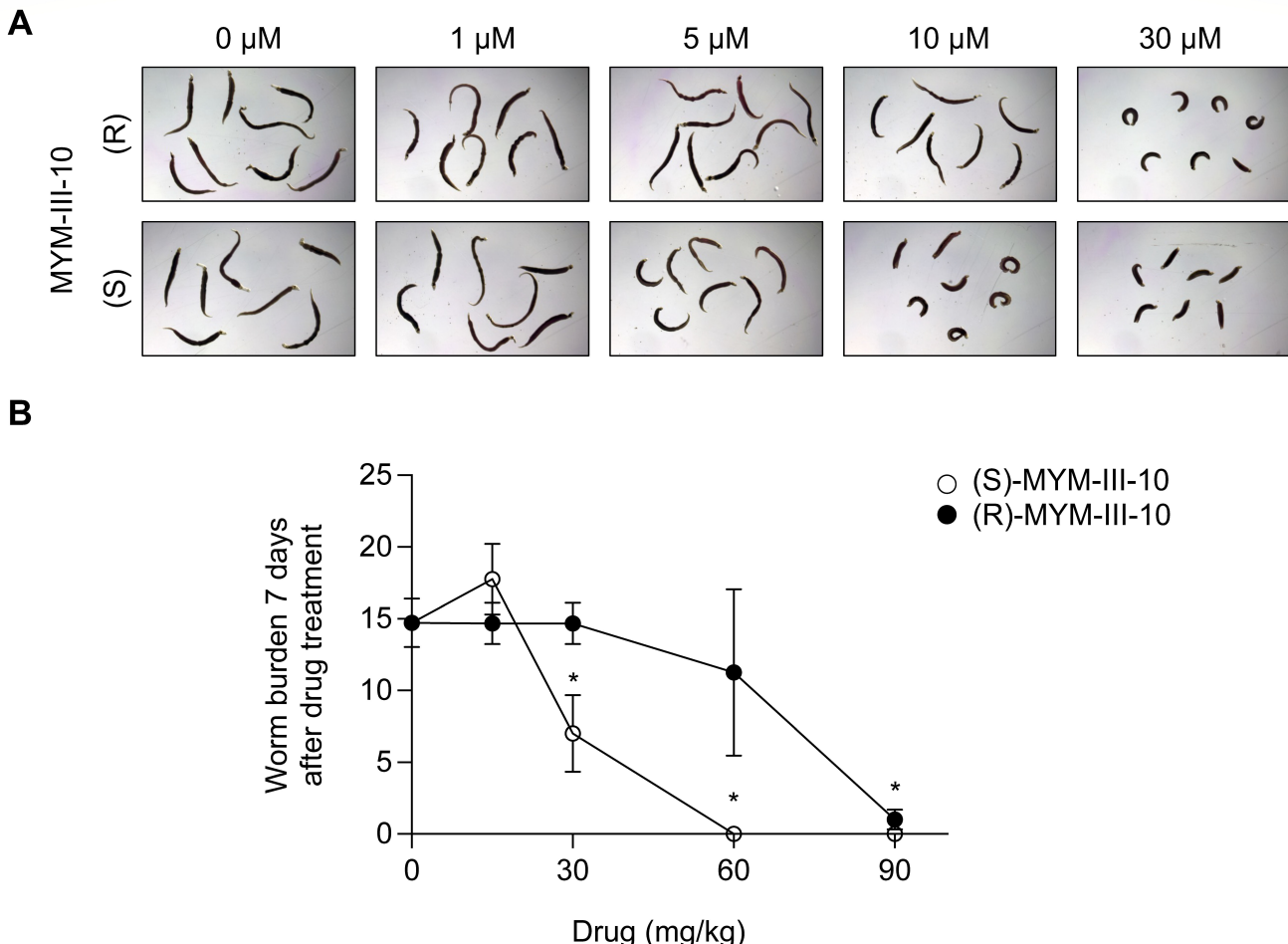


**FIG 4** Antischistosomal activity of MYM-III-10 enantiomers. (A) *In vitro* effect of purified (R)- and (S)-MYM-III-10 enantiomers on adult worms (14-hour incubation). (B) *In vivo* efficacy of each MYM-III-10 enantiomer against adult parasites. Mice (*n* = 3–7 per drug treatment, depending on compound availability) were dosed with various amounts of each compound 6 weeks post-infection and euthanized 1 week later to assess worm burden. Symbols denote mean ± standard error. Significance of differences between drug treatments and DMSO control is reflected by \**P* < 0.05 (Mann–Whitney *U* test).

device and attempt to escape during the assay. Therefore, while this compound does not have pronounced sedating activity, it does appear to have other psychoactive effects.

In order to investigate the action of the two hit compounds, MYM-III-10 and MYM-V-56, on host targets, we performed a series of binding and functional assays. Binding assays revealed that both compounds displace diazepam radioligand from rat brain membrane preparations with similar potency as MCLZ. Therefore, both MYM-III-10 and MYM-V-56 appear to have affinity for host GABA<sub>A</sub>Rs (Fig. 6A), even if they are less sedating *in vivo*. Similarly, both compounds have similar activity in functional assays measuring PAM activity at GABA<sub>A</sub>Rs, stimulating peak currents measured from  $\alpha$ 1 $\beta$ 2 $\gamma$ 2 GABA<sub>A</sub> channels recombinantly expressed in mammalian CHO-K1 cells (Fig. 6B).

Given the increased polarity of MYM-III-10 (ClogP 1.01) relative to MCLZ (ClogP 2.39), we hypothesized that the decrease in sedation observed with MYM-III-10 treatment may be due to less compound crossing the blood–brain barrier. This was confirmed by measuring levels of drug in serum and brain tissue. Mice were treated orally with either MCLZ or MYM-III-10 as in the antischistosomal and rotarod assays and then euthanized to harvest whole blood and dissect brains from each animal. Drug levels were measured in each sample, revealing that indeed MCLZ but not MYM-III-10 accumulated in the brain tissue. This was not due to a lack of MYM-III-10 bioavailability, since this compound was found at high levels in the serum (Fig. 6C).

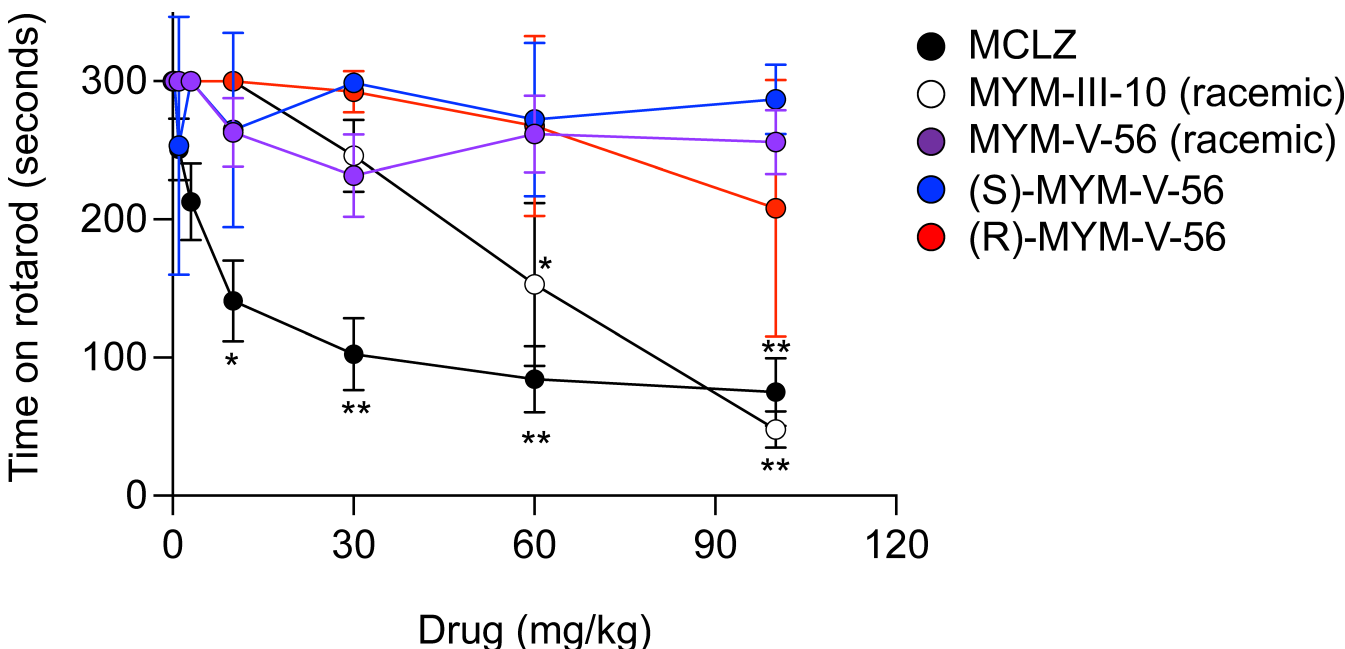


**FIG 5** Sedating activity of antischistosomal benzodiazepines. Sedation was measured by ability to complete the rotarod test. Mice (between  $n = 4$ –5 per drug treatment, depending on compound availability) were dosed with varying amounts of test compound or vehicle control and assayed for their ability to run on the device for 3 minutes (symbols denote mean  $\pm$  standard error, black = MCLZ, white = MYM-III-10, purple = MYM-V-56, blue = (S)-MYM-V-56, and red = (R)-MYM-V-56. Significance of differences between drug treatments and DMSO control is reflected by \* $P < 0.05$  and \*\* $P < 0.01$  (paired t-test).

An explanation for the lack of MYM-V-56 sedation is less straightforward. Like MCLZ, it is a relatively non-polar compound ( $\text{ClogP} 2.42$ ) that would be expected to cross the blood-brain barrier. We reasoned that activity at receptors other than  $\text{GABA}_\text{A}$ Rs may mediate the psychoactive effects of this compound and submitted MYM-V-56 to a panel of 44 different binding and functional assays (Eurofins Safety Screen44 Panel; Table S2) to profile activity against a range of targets at a concentration of 10  $\mu\text{M}$ . These results confirmed that MYM-V-56 binds  $\text{GABA}_\text{A}$ Rs, but no other assay showed significant displacement of radioligand. MYM-V-56 was also submitted to the National Institutes of Health (NIH) National Institute of Mental Health (NIMH) Psychoactive Drug Screening Program (PDSP) (32), where binding assays were performed against 46 different targets. These data also did not show significant displacement of radioligand at any of the targets screened (Table S2). Therefore, future work will be required to elaborate on the mammalian targets of MYM-V-56 and minimize the psychoactive effects of this compound.

## DISCUSSION

It has been known for over 40 years that certain benzodiazepines exhibit antischistosomal activity (27), including the compound MCLZ, which was curative in a human clinical trial (12). While several studies have investigated additional MCLZ derivatives (21, 33, 34), until now it has not been shown that it is possible to develop a benzodiazepine that retains antiparasitic effects *in vivo* but lacks sedative effects.

The two compounds that resulted from this screen, MYM-V-56 and MYM-III-10, both contain modifications at the C3 position of MCLZ. This position was particularly interesting for exploration given the comparison of MCLZ and the anxiolytic/antiseizure medication clonazepam. Clonazepam is identical to MCLZ, except it lacks a methyl group at the C3 position. This difference makes clonazepam approximately three times *less* potent on schistosomes (causing paralysis at 10  $\mu\text{M}$ , compared to 3  $\mu\text{M}$  for MCLZ), but it binds host  $\text{GABA}_\text{A}$ Rs with approximately three times *higher* potency (displacement of diazepam radioligand with a  $K_i = 0.82$  nM, compared to 2.4 nM for MCLZ) (21,

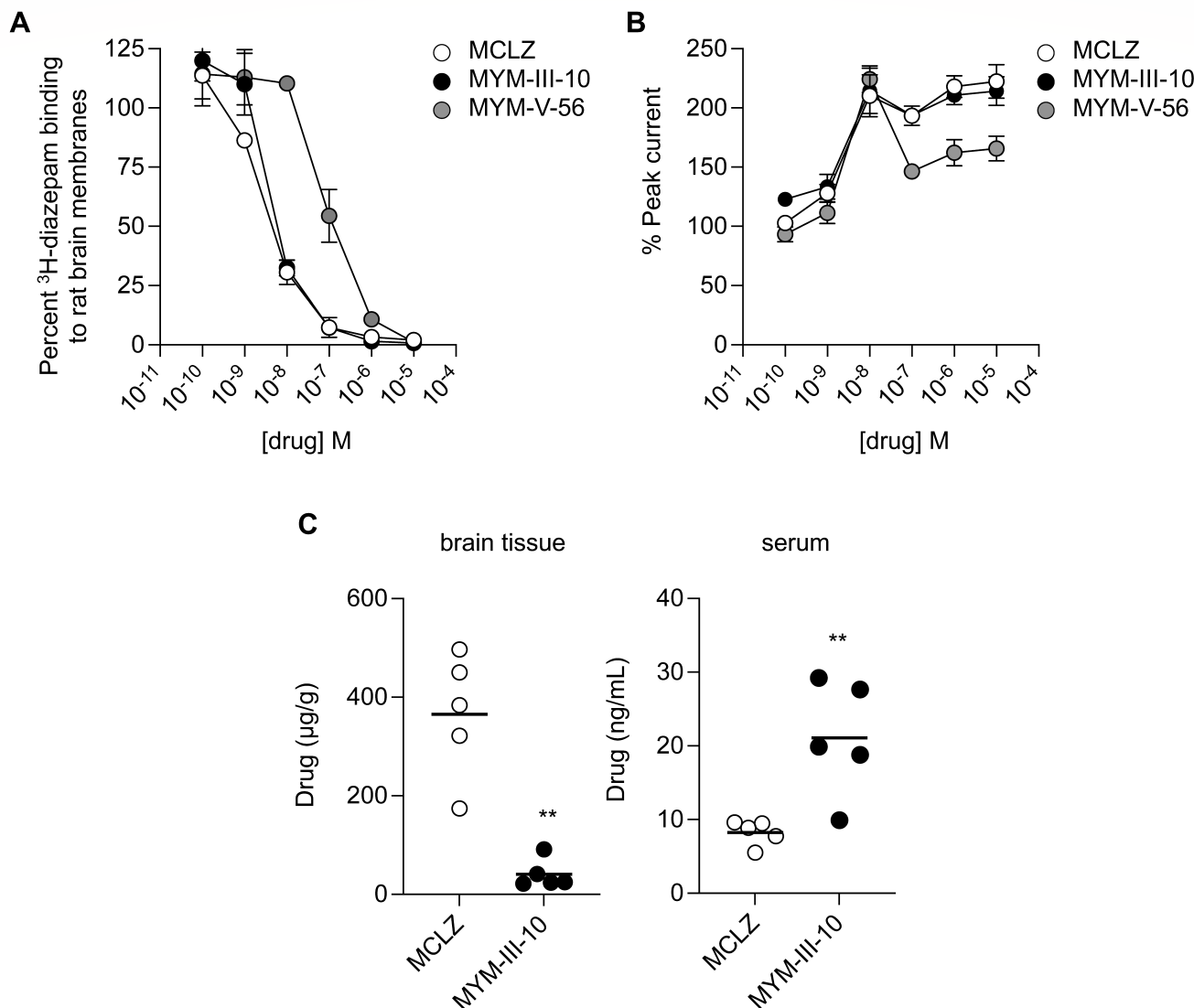


**FIG 6** Activity of antischistosomal benzodiazepines on mammalian central nervous system (CNS) targets. (A) Affinity for CNS GABA<sub>A</sub>Rs was measured by assaying the ability of MCLZ (open symbols), MYM-III-10 (black symbols), or MYM-V-56 (gray symbols) to displace <sup>3</sup>H-diazepam radioligand from rat brain membranes. Symbols denote mean ± standard error of *n* = 3 replicates. (B) PAM activity of MCLZ, MYM-III-10, and MYM-V-56 was measured by recording GABA-evoked Cl<sup>-</sup> currents from α1β2γ2 GABA<sub>A</sub> channels recombinantly expressed in mammalian CHO-K1 cells. All three compounds displayed PAM activity. Symbols denote mean ± standard error of *n* = 3 replicates. (C) Levels of MYM-III-10 and MCLZ in either mouse brain tissue or serum were measured by HPLC following oral dosing (100 mg/kg). Symbols reflect drug measurements from individual mice (between *n* = 5 mice per condition). Significance of differences between drug treatments and DMSO control is reflected by \*\**P* < 0.01 (Mann-Whitney *U* test).

34). Other pairings with a functional group on the benzodiazepine C3 position can also slightly impair GABA<sub>A</sub>R binding affinity, such as nordazepam ( $K_i$  = 8.9 nM) versus oxazepam which has a C3 hydroxy group ( $K_i$  = 38 nM) (35). While substitution of the MCLZ methyl group with a hydroxyl group (MYM-III-10) or fluorine (MYM-V-56) was tolerated, larger substitutions lost or attenuated antiparasitic activity [e.g., putting two methyl groups at the C3 position (MYM-II-74), increasing the length of the alkyl chain to an ethyl group (MYM-V-19), or adding an ester (MYM-II-83)]. Putting a ketone at this position (MYM-V-50) also resulted in a loss of activity, which is somewhat expected since stereochemistry is known to impact antischistosomal activity (27), and this modification results in a loss of the chiral stereocenter at the C3 position. Future work elaborating on

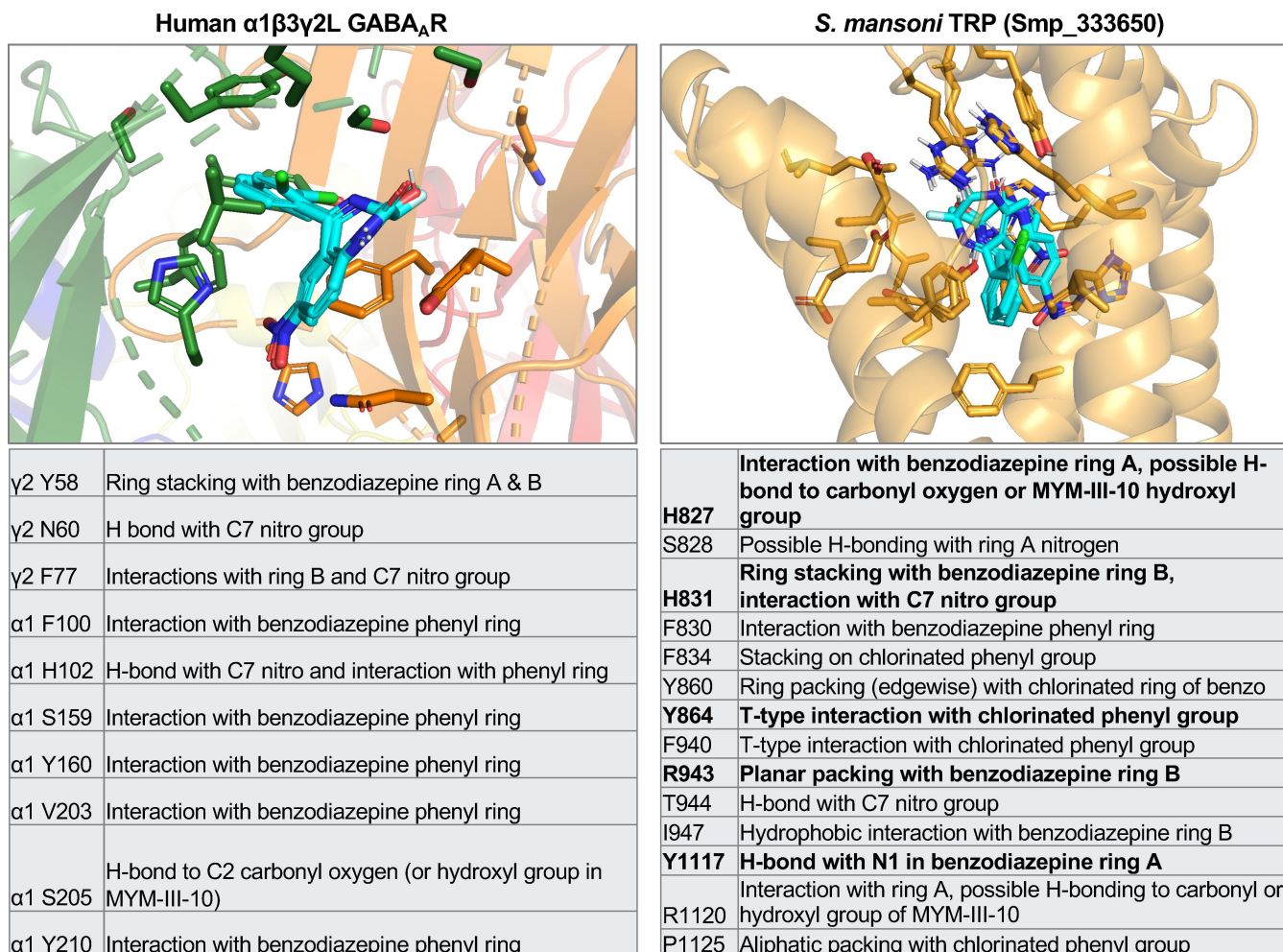


**FIG 7** Modeled benzodiazepine interactions with host and parasite receptors. Left: MCLZ, (S)-MYM-V-56 and (S)-MYM-III-10 (cyan) docked into the benzodiazepine binding pocket of the human  $\alpha 1\beta 3\gamma 2L$  GABA<sub>A</sub> receptor (cryo-EM structure 6HUP, reference (40). y2 subunit is shown in green, α1 subunit in orange. Right: the same three benzodiazepines docked into the VSLD cavity of the *S. mansoni* TRP Smp\_333650 [alphaFold structure prediction for A0A5K4FCC0, (14)]. Bottom: predicted potential interactions between ligands and amino acid side chains. Bold = amino acids experimentally validated by mutagenesis studies in reference (14). Docking scores are provided in Supplemental File S5, and ligand–side chain interactions are elaborated upon in Supplemental File S6. PyMOL session files containing the ligands docked into both the human GABA<sub>A</sub>R (6HUP) and AlphaFold model of the *S. mansoni* TRP channel Smp\_333650 can be accessed at <https://doi.org/10.5281/zenodo.10697837>.

the structure–activity relationship of compounds with modifications at this position may further optimize the antischistosomal activity of this series.

The recent finding that MCLZ acts as an agonist on a schistosome TRP channel enables modeling of the chemical series screened in this study within the benzodiazepine binding pocket of the putative parasite target and a comparison of the structure–activity relationship (SAR) at human receptors (Fig. 7; Supplemental File S5 and S6). Interestingly, even though the worm TRP channel and human GABA<sub>A</sub>Rs belong to distinct classes of ion channels with little structural similarity, several common positions on the benzodiazepine ring system are required for activity at both targets. It has been well established that the chirality of the C3 position and presence of electron-withdrawing groups at the C7 and phenyl C2' positions was required for benzodiazepine binding affinity to GABA<sub>A</sub>Rs (35–39), and these interactions were confirmed by resolving the structure of diazepam- and alprazolam-bound  $\alpha 1\beta 3\gamma 2L$  GABA<sub>A</sub>Rs (40). As expected, MCLZ docked into this binding pocket adopts a similar pose interacting with side chains known to mediate binding affinity (Fig. 7). However, our SAR data show

that similar criteria exist at these same positions of the benzodiazepine molecule for antiparasitic effects. The importance of the nitro functional group at the C7 position is clear from our chemical series; removing the nitro so that the C7 is unmodified causes a loss of activity (MYM-V-03), as does replacing the nitro with another functional group (MYM-IV-01, MYM-IV-02, MYM-IV-03, MYM-IV-12, and MYM-IV-63). This is likely due to the electrostatic interactions between the nitro group and tyrosine and histidine side chains in the binding pocket [Fig. 7; (14)]. Similarly, the C2' position was known to be critical due to the inactivity of nitrazepam (21) and modeled interaction with Y864 supported by mutagenesis experiments (14). The importance of the chlorine at this position is demonstrated by the reduced activity of MYM-V-58, which is identical to the active MYM-V-56 but contains a fluorine at the C2' position. Finally, the compound MYM-II-53, which contains a methyl group on the N1 position, was inactive in our screen and was also inactive against the recombinantly expressed TRP channel Smp\_333650 (14). This compound was also inactive on schistosomes in reference (34), along with numerous other N1-alkylated compounds. The patent filing by Roche [US4031078A, (27)] for anthelmintic benzodiazepine derivatives stated that the N1 could contain a lower alkyl group, but this is not supported by our data or those in references (14, 34). This is one distinction compared to the criteria for GABA<sub>A</sub>R affinity, where N1 alkyl groups are tolerated (e.g., N1 methyl on diazepam). Finally, we note that, given the conservation of the putative TRP target of benzodiazepines in *S. haematobium*, it would be expected that the compounds MYM-III-10 and MYM-V-56 would also be effective against this species (14).

While both MYM-III-10 and MYM-V-56 were less sedating than MCLZ, both of these compounds still retained PAM activity against GABA<sub>A</sub>Rs that would be expected to confer sedation (Fig. 5 and 6). So why were MYM-III-10 and MYM-V-56 not as sedating as MCLZ? For MYM-III-10, an explanation may relate to pharmacokinetic properties of this molecule, since it is more polar with a hydroxyl group at the C3 position. A lower ClogP would be expected to have less blood–brain barrier penetration and sedation (41), which is indeed what is observed when levels of this compound were measured in brain tissue (Fig. 6C).

While there is a plausible explanation for why MYM-III-10 is much less sedating than MCLZ despite GABA<sub>A</sub>R affinity, it is less clear why MYM-V-56 is not sedating. The activity of MYM-V-56 on GABA<sub>A</sub>Rs does differ slightly from MCLZ and MYM-III-10. MYM-V-56 does not have quite as potent affinity as these two compounds for the central benzodiazepine binding site in radioligand binding assays (Fig. 6A), but does still bind with relatively high affinity. MYM-V-56 also displays potent PAM activity at recombinantly expressed GABA<sub>A</sub>Rs (Fig. 6B), even though receptors desensitize at higher concentrations. From these data, we may still expect that MYM-V-56 would be sedating, but this was not the case in the rotarod assay even at doses up to 100 mg/kg (Fig. 5). However, from observing these mice, it was clear that MYM-V-56 does have unique psychoactive effects (Supplemental File S4). We designed our behavioral experiments to use the rotarod test anticipating sedation and not hyperactivity, given the large body of prior work on benzodiazepines. However, a quantitative description of this hyperactivity would be better measured with a different assay such as the open field test. Nevertheless, these mice were clearly hyperactive, indicating that MYM-V-56 may have activity on targets other than GABA<sub>A</sub>Rs or GABA<sub>A</sub>Rs with different subunit compositions than the typical  $\alpha 1$ -containing channels that cause sedation (e.g.,  $\alpha 2$ -containing channels that mediate anxiolytic effects). The identity of what those receptors may be is not clear and remains a topic for future investigation (Table S2). Indeed, while the rotarod data showing a lack of sedation appears promising for this compound, the distinct psychoactive effects observed would likely not be acceptable for further development. Exploration of additional molecules with C3 modifications using other behavioral tests is warranted to determine whether related compounds (e.g., different halogens or other electrophilic groups) would have the same effect.

The structure-activity relationship of MCLZ derivatives explored in this study, as well as the comparative modeling of the host and parasite receptors and the identification of two new lead molecules, will advance benzodiazepines as promising candidates for development as new antischistosomal therapies. This class of compounds displays excellent antiparasitic activity, through mechanisms distinct from the existing monotherapy, PZQ. Benzodiazepines also have an established track record as highly prescribed drugs (>5% of adults in the United States) with known safety profiles (42). The primary barrier so far to developing these compounds to treat schistosomiasis has been dose-limiting sedation, which we demonstrate can be reduced or eliminated in a murine model.

## MATERIALS AND METHODS

### Chemical synthesis

MCLZ was purchased from Anant Pharmaceuticals and verified as greater than 99% pure by HPLC. For HPLC experiments, a MCLZ reference standard was purchased from Sigma Aldrich (catalog number M-197-1ML). The reactions were performed in round-bottom flasks with magnetic stir bars under an argon atmosphere or air condition. Organic solvents were purified when necessary by standard methods or purchased from Sigma-Aldrich Chemicals. Reagents and other chemicals were purchased from either Sigma-Aldrich, Oakwood Chemical, Alfa Aesar, Matrix Scientific, Admiral Chemical Company, or Acros Organic. The progress of reactions was visualized with thin layer chromatography (TLC) plates from Dynamic Adsorbents, Inc. under a UV light. LCMS 2020 was used to monitor some reactions. Flash column chromatography was done for purification of some analogs on silica gel (230–400 mesh, Dynamic Adsorbents). A normal phase Agilent HPLC was used to determine the ratio of optically active enantiomers as well as to determine the percentage. The <sup>1</sup>H nuclear magnetic resonance (NMR) and <sup>13</sup>C NMR spectra were obtained on Bruker Spectrospin 500 MHz instrument in CDCl<sub>3</sub>, and chemical shifts were reported in δ (ppm). Multiplicities are represented as follows: singlet (s), broad signal (br), doublet (d), triplet (t), quartet (q), dd (doublet of doublets), and multiplet (m). The technique employed for HRMS was carried out on an LCMS-IT-TOF (liquid chromatograph mass spectrometer with ion trap and time-of-flight technologies) at the Milwaukee Institute for Drug Discovery in the Shimadzu Laboratory for Advanced and Applied Analytical Chemistry. Detailed synthesis methods, reaction schemes, and NMR spectra for compounds shown in Fig. 1 are provided in Supplemental File S1.

### Purification of enantiomers

MYM-III-10 and MYM-V-56 enantiomers were purified by preparative HPLC. The (R) and (S) enantiomers of MYM-III-10 were separated by using an isocratic mixture of 88% n-hexane and 12% ethanol as the mobile phase in an HPLC system consisting of a quaternary pump, autosampler, and a diode array detector (DAD). The method time was set for 55 minutes. A chiral preparative HPLC column, 5 μm, 25 cm × 21.1 mm, was used for separating the enantiomers. The first fraction (*R* isomer) for MYM-III-10 was collected from 35.2 to 40.2 minutes, and the second fraction was collected from 45.5 to 50 minutes. Approximately, 15 mL of sample was collected for each fraction after each injection. The fractions were evaporated separately just after collection and dried. Compounds were then analyzed by NMR. The DAD wavelength range was set at 200–400 nm. A 254-nm wavelength was used for relative % area determination. The flow rate was set at 21 mL/min.

The (R) and (S) enantiomers of MYM-V-56 were separated using the same method but set for 25 minutes. The first fraction (*R* isomer) for MYM-V-56 was collected from 19.5 to 21.2 minutes, and the second fraction was collected from 22.4 to 23.4 minutes. Approximately, 15 mL of sample was collected for each fraction after each injection. The fractions were evaporated separately just after collection, dried, and analyzed by NMR.

To confirm the absolute configuration of MYM-V-56, the X-ray crystal structure of the first fraction was determined, and it turned out to be the (R) configuration, indicating the other enantiomer is (S)-configuration. A clear colorless chunk crystal of dimensions  $0.236 \times 0.185 \times 0.080$  mm was mounted on a MiteGen MicroMesh using a small amount of Cargille Immersion Oil. Data were collected on a Bruker three-circle platform diffractometer equipped with a PHOTON II CPAD detector. The crystals were irradiated using a  $1\text{-}\mu\text{s}$  microfocus  $\text{CuK}_\alpha$  source ( $\lambda = 1.54178$ ) with Montel optics. Data were collected at room temperature ( $20^\circ\text{C}$ ), and the unit cell was initially refined using *APEX3* (v2015.5–2) (43). Data reduction was performed using *SAINT* (v8.34A) and *XPREP* (v2014/2) (Bruker AXS Inc.). Corrections were applied for Lorentz, polarization, and absorption effects using *SADABS* (v2014/2), and the structure was solved and refined with the aid of *SHELXL-2014/7* (Bruker AXS Inc.). The full-matrix least-squares refinement on  $R^2$  included atomic coordinates and anisotropic thermal parameters for all non-H atoms. Hydrogen atoms were located from the difference electron density maps and added using a riding model.

### *In vitro* antischistosomal activity assays

Female Swiss Webster mice were infected with NMRI strain *S. mansoni* by the NIH-National Institute of Allergy and Infectious Diseases (NIAID) Schistosomiasis Resource Center. Briefly, infectious cercariae were shed from *Biomphalaria glabrata* snails. A total of 180 parasites were then used to infect each mouse, submerging the tail in water containing the appropriately titrated amount of cercariae. After 6–7 weeks, parasites mature to adults and were harvested for experiments following euthanization of the mouse host by  $\text{CO}_2$  asphyxiation and cervical dislocation. Adult schistosomes were harvested from the mesenteric vasculature and placed in culture media consisting of high-glucose Dulbecco's modified Eagle medium supplemented with 5% fetal calf serum, penicillin-streptomycin (100 units/mL), HEPES (25 mM), and sodium pyruvate (1 mM) and cultured at  $37^\circ\text{C}/5\%$   $\text{CO}_2$ .

Six to eight worms were treated with either dimethyl sulfoxide (DMSO) control (0.1% vol/vol) or test compounds listed in Table S1 for 14 hours at  $37^\circ\text{C}/5\%$   $\text{CO}_2$  prior to observing phenotypes. Worms were visually observed on a Zeiss Stemi 305 Stereo Microscope to assess changes in morphology, and images were captured on an Axiocam 208 color camera. For motility experiments, serotonin (5-HT) was added at  $250\text{ }\mu\text{M}$  to increase worm movement at least 1 hour prior to imaging on an ImageXpress Nano (Molecular Devices). Time-lapse recordings were acquired for a single, unpaired male worm in each well (15-second videos at a rate of four frames/second) using a 2 $\times$  objective. Movement was analyzed using the wrmXpress package (25). Unpaired male worms were chosen rather than paired worms or female worms, because this analysis package measures movement of pixels. Paired worms tend to transiently unpair and then repartner, occasionally doubling the amount of observable worms in the field of view whenever the female separates from inside the male. Additionally, female worms (whether paired or unpaired) tend to lay eggs within the well which also are detected as moving pixels and introduce unreliable motility values. Significance for motility assays was determined by unpaired *t*-tests, and *P* values are denoted in figure legends as less than 0.05 or 0.01.

### *In vivo* antischistosomal activity assays

For hepatic shift assays, female mice harboring 7-week-old *S. mansoni* infections were administered either DMSO control, MCLZ, or test compound solubilized in vegetable oil (0.25 mL) by oral gavage and then euthanized as outlined above ( $\text{CO}_2$  asphyxiation followed by cervical dislocation) 3 hours later. Worms were dissected from the liver and mesenteries, and the percentage of worms in each location was calculated. An image illustrating the relevant mouse anatomy in this assay and the direction of the hepatic shift from the mesenteric vasculature to the liver is shown in Fig. 2A, reproduced from reference (29). For longer-term assays measuring curative activity of drugs, compounds

were administered orally to mice harboring 6-week-old *S. mansoni* infections. Mice were euthanized 1 week later, and the parasite burden for each mouse was counted. Parasite burden reflects counts of paired adult worms. Significance was determined using the Mann–Whitney *U* test. To assess the curative effects of compounds on juvenile, liver stage parasites, mice harboring 4-week-old *S. mansoni* infections were dosed orally with test compound and euthanized at 7 weeks to count parasite burden. While we strove to have at least  $n = 5$  mice per condition, the number of animals treated with drug was limited by the amount of test compound that could be synthesized and purified for a given experiment – especially for experiments requiring higher doses of drug. Mouse numbers are provided in figure legends describing respective experiments.

### Rotarod assay for sedation

Six-week-old female Swiss Webster mice were chosen for study since this matches the strain used in the parasite assays. Uninfected mice were ordered from Taconic or Charles River and trained to perform the rotarod test using a IITC Life Science rotarod device with the following settings: 20 RPM max speed, 20 ramp speed, and 300-second duration test. Mice were run five at a time and only used for drug assays if they were capable of completing the training and able to run on the device for the entire 300 seconds. Mice were then dosed with test compounds by oral gavage and tested on the rotarod device after 5 minutes. Results were analyzed by paired *t*-tests comparing no-drug to drug-treated runs.

### Detection of MCLZ and MYM-III-10 in brain and serum

Six-week-old female Swiss Webster mice were dosed with MCLZ or MYM-III-10 (100 mg/kg) as described in the antischistosomal assays and then euthanized after 10 minutes by CO<sub>2</sub> asphyxiation. This time period corresponds to the window within which we observe sedation in rotarod assays. Whole blood samples were collected from each mouse and allowed to clot at room temperature for 15 minutes. Serum was separated by centrifugation at 2,000  $\times g$  for 10 minutes. The skull was opened with scissors, and all brain tissue was removed. Both samples were frozen at -80°C until ready for analysis by HPLC.

Preparing samples for HPLC brain tissue homogenized with BeadBug microtube homogenizer and the solid phase extraction procedure was carried out on Hypersep C18 cartridges. Separations were obtained on Shimadzu HPLC System with Waters Symmetry C18 column (150  $\times$  3.9-mm id, 5  $\mu$ m) kept at 30°C. The mobile phase was composed of a mixture of MeOH (65% vol/vol) + 0.1% formic acid and a ultrapure water (35% vol/vol) + 0.1% formic acid. The flow rate was set at 0.5 mL/min. Detection was carried out on a Shimadzu Diode Array Detector SPD-M20A at 254 nm. Spiked-in MCLZ was used as an internal standard for MYM-III-10 treated samples and vice versa.

### Binding and functional assays

MYM-V-56 binding was assessed by two panels of assays. The Safety Screen 44 Panel was performed by Eurofins Pharma Discovery. Per vendor recommendations, each assay was performed using 10  $\mu$ M of MYM-V-56 in technical duplicates. MYM-V-56 (10  $\mu$ M) binding to receptors in the NIMH PDSP was performed in technical quadruplicate per SOPs in the PDSP assay protocol book, which can be found at <https://pdsp.unc.edu/pdspweb/>.

### Modeling benzodiazepine binding to TRP and GABA<sub>A</sub>Rs

Targets were obtained from public structure repositories. GABA<sub>A</sub>R coordinates were taken from the Research Collaboratory for Structural Bioinformatics Protein Data Bank (RSCB PDB) accession 6HUP for a cryo-EM derived structure in its diazepam-bound state. The AlphaFold model AF-A0A5K4FCC0-F1-model provided starting coordinates for the *S. mansoni* TRP channel Smp\_333650. Structure models were prepared for docking using the DockPrep utility of ChimeraX v1.7 (44) to fill in missing atoms, add hydrogens, and

assign partial charges (AMBER ff14SB) and exported in mol2 formats. SMILES for the benzodiazepine chemical series were generated using ChemDraw. Library preparation utilities fixpka (QUACPAC v2.1.2.1), OMEGA2 v4.1.1.1, and molcharge (QUACPAC v2.1.2.1) were used to assign protonation states, build energetically reasonable starting 3D conformers for docking, and assign partial charges (Merck Molecular Force Field, MMFF), respectively (OpenEye Scientific, Cadence Molecular Sciences, Inc.). Single conformations were exported in mol2 format for docking. Docking was performed using the program Gnina v1.0 (45). To localize the search space in docking GABA<sub>AR</sub>, the binding pocket was specified based on the position of diazepam using the autobox option with a bounding box of 10 Angstroms. No sidechain flexibility was allowed for docking into the GABA<sub>AR</sub>. For the schistosome TRP channel, the site center was determined using the most probable site in the voltage-sensor-like structure (VSLD) domain using the prediction tool p2rank (46). Due to steric restrictions within the putative binding pocket of the TRP channel, sidechain flexibility was enabled for pocket residues H827, H831, Y864, E867, E868, D893, F940, R943, H946, I947, Y1117, and R1120. For both targets, extensive sampling was achieved using an exhaustiveness parameter of 64. Convolutional neural network (CNN) scoring was used for rescoring final poses by setting cnn\_scoring option to "rescore." For CNN-based pose scoring, the "crossdock\_default2018" model was selected. Docking poses were inspected and images created using PyMOL v2.5.4 (Schrodinger, LLC). PyMOL session files (.pse) containing the ligands docked into both the human GABA<sub>AR</sub> (6HUP) and AlphaFold model of the *S. mansoni* TRP channel Smp\_333650 can be accessed at <https://doi.org/10.5281/zenodo.10697837>.

## ACKNOWLEDGMENTS

We acknowledge the UW-Milwaukee Shimadzu Laboratory for Advanced and Applied Analytical Chemistry and support from the Milwaukee Institute of Drug Discovery and the University of Wisconsin-Milwaukee Research Foundation. Schistosome-infected mice were provided by the NIH-NIAID Schistosomiasis Resource Center for distribution through BEI Resources, NIH-NIAID Contract HHSN272201700014I. Receptor binding profile for MYM-V-56 was generously provided by the NIMH's PDSP, contract # HHSN-271-2018-00023-C (NIMH PDSP). We thank Jonathan Marchant for sharing the pdb file of MCLZ docked into Smp\_333650, facilitating in silico modeling of the compounds reported in this study.

This work was supported by funding from NIH-NIAID R21AI146540 (J.D.C.) and a University of Wisconsin System Regent Scholar Award (J.D.C. and J.M.C.). J.D.C. is supported by funding from the University of Wisconsin-Madison Global Health Institute. J.M.C. is also supported by R01DA011792, R01DA043204 and R01NS076517, Office of Naval Research grant N00014-15 WX-0-0149, and NSF Chemistry Research Instrumentation Program award #1625735.

## AUTHOR AFFILIATIONS

<sup>1</sup>Department of Chemistry and Biochemistry, University of Wisconsin-Milwaukee, Milwaukee, Wisconsin, USA

<sup>2</sup>Milwaukee Institute of Drug Discovery, University of Wisconsin-Milwaukee, Milwaukee, Wisconsin, USA

<sup>3</sup>Department of Cell Biology, Neurobiology and Anatomy, Medical College of Wisconsin, Milwaukee, Wisconsin, USA

<sup>4</sup>Department of Pathobiological Sciences, University of Wisconsin-Madison, Madison, Wisconsin, USA

<sup>5</sup>UW Carbone Cancer Center, University of Wisconsin-Madison, Madison, Wisconsin, USA

<sup>6</sup>Department of Chemistry, University of Wisconsin Oshkosh, Oshkosh, Wisconsin, USA

## AUTHOR ORCIDs

Mostafa Zamaniyan  <http://orcid.org/0000-0001-9233-1760>

John D. Chan  <http://orcid.org/0000-0003-4986-972X>

## FUNDING

Funder	Grant(s)	Author(s)
HHS   NIH   National Institute of Allergy and Infectious Diseases (NIAID)	R21AI146540	John D. Chan

## AUTHOR CONTRIBUTIONS

Md Yeonus Mian, Conceptualization, Data curation, Formal analysis, Investigation, Methodology, Writing – original draft, Writing – review and editing | Dishary Sharmin, Conceptualization, Data curation, Investigation, Methodology | Prithu Mondal, Investigation, Methodology | Jawad Bin Belayet, Investigation, Methodology | M. Mahmun Hossain, Investigation, Methodology | Paul McCusker, Investigation, Methodology, Writing – review and editing | Kaelyn T. Ryan, Formal analysis, Investigation, Methodology, Software, Writing – original draft, Writing – review and editing | Alexander Y. Fedorov, Data curation, Formal analysis, Investigation, Methodology, Writing – original draft | Heather A. Green, Investigation, Methodology, Writing – review and editing | Spencer S. Erickson, Conceptualization, Data curation, Formal analysis, Investigation, Methodology, Software, Validation, Visualization, Writing – original draft | Mostafa Zamanian, Conceptualization, Project administration, Supervision, Writing – original draft, Writing – review and editing | V. V. N. Phani Babu Tiruveedhula, Conceptualization, Investigation, Methodology, Project administration | James M. Cook, Conceptualization, Formal analysis, Funding acquisition, Methodology, Project administration, Supervision, Writing – review and editing | John D. Chan, Conceptualization, Data curation, Formal analysis, Funding acquisition, Investigation, Methodology, Project administration, Resources, Supervision, Validation, Visualization, Writing – original draft, Writing – review and editing

## ETHICS APPROVAL

All animal work was carried out with the oversight and approval of UW-Madison Research Animal Resources and Compliance (RARC), adhering to the humane standards for the health and welfare of animals used for biomedical purposes defined by the Animal Welfare Act and the Health Research Extension Act. Experiments were approved by the UW-Madison School of Veterinary Medicine Institutional Animal Care and Use Committee (IACUC) (approved protocol #V006353-A08).

## ADDITIONAL FILES

The following material is available [online](#).

### Supplemental Material

**Supplemental File S1 (AAC00369-24-s0001.pdf).** Supporting data on synthesis and purification of meclonazepam derivatives.

**Supplemental File S2 (AAC00369-24-s0002.mp4).** Video of mice treated with vehicle control.

**Supplemental File S3 (AAC00369-24-s0003.mp4).** Video of mice treated with MCLZ.

**Supplemental File S4 (AAC00369-24-s0004.mp4).** Video of mice treated with MYM-V-56.

**Supplemental File S5 (AAC00369-24-s0005.xlsx).** Scores for benzodiazepines docked into the human GABA<sub>A</sub>R and *S. mansoni* TRP channel.

**Supplemental File S6 (AAC00369-24-s0006.pdf).** LigPlot visualization of meclonazepam binding in the human GABA<sub>A</sub>R and *S. mansoni* TRP channel.

**Supplemental File S7 (AAC00369-24-s0007.docx).** Legends for supplemental material.

**Supplemental Table S1 (AAC00369-24-s0008.xlsx).** Structures of test compounds.**Supplemental Table S2 (AAC00369-24-s0009.xlsx).** Binding of MYM-V-56 to human receptors.**REFERENCES**

- Lo NC, Bezerra FSM, Colley DG, Fleming FM, Homeida M, Kabatereine N, Kabole FM, King CH, Mafe MA, Midzi N, et al. 2022. Review of 2022 WHO guidelines on the control and elimination of schistosomiasis. *Lancet Infect Dis* 22:e327–e335. [https://doi.org/10.1016/S1473-3099\(22\)00221-3](https://doi.org/10.1016/S1473-3099(22)00221-3)
- Fukushige M, Chase-Topping M, Woolhouse MEJ, Mutapi F. 2021. Efficacy of praziquantel has been maintained over four decades (from 1977 to 2018): a systematic review and meta-analysis of factors influence its efficacy. *PLoS Negl Trop Dis* 15:e0009189. <https://doi.org/10.1371/journal.pntd.0009189>
- Berger DJ, Crellin T, Lamberton PHL, Allan F, Tracey A, Noonan JD, Kabatereine NB, Tukahebwa EM, Adrisko M, Holroyd N, Webster JP, Berriman M, Cotton JA. 2021. Whole-genome sequencing of *Schistosoma mansoni* reveals extensive diversity with limited selection despite mass drug administration. *Nat Commun* 12:4776. <https://doi.org/10.1038/s41467-021-24958-0>
- Ismail MM, Taha SA, Farghaly AM, el-Azony AS. 1994. Laboratory induced resistance to praziquantel in experimental schistosomiasis. *J Egypt Soc Parasitol* 24:685–695.
- Fallon PG, Doenhoff MJ. 1994. Drug-resistant schistosomiasis: resistance to praziquantel and oxamniquine induced in *Schistosoma mansoni* in mice is drug specific. *Am J Trop Med Hyg* 51:83–88. <https://doi.org/10.4269/ajtmh.1994.51.83>
- Le Clec'h W, Chevalier FD, Mattos ACA, Strickland A, Diaz R, McDew-White M, Rohr CM, Kinung'hi S, Allan F, Webster BL, Webster JP, Emery AM, Rollinson D, Djiray AG, Al Mashikhi KM, Al Yafae S, Idris MA, Moné H, Mouahid G, LoVerde P, Marchant JS, Anderson TJC. 2021. Genetic analysis of praziquantel response in schistosome parasites implicates a transient receptor potential channel. *Sci Transl Med* 13:eabj9114. <https://doi.org/10.1126/scitranslmed.labj9114>
- Ismail M, Botros S, Metwally A, William S, Farghally A, Tao LF, Day TA, Bennett JL. 1999. Resistance to praziquantel: direct evidence from *Schistosoma mansoni* isolated from Egyptian villagers. *Am J Trop Med Hyg* 60:932–935. <https://doi.org/10.4269/ajtmh.1999.60.932>
- Melman SD, Steinauer ML, Cunningham C, Kubatko LS, Mwangi IN, Wynn NB, Mutuku MW, Karanja DMS, Colley DG, Black CL, Secor WE, Mkoi GM, Loker ES. 2009. Reduced susceptibility to praziquantel among naturally occurring Kenyan isolates of *Schistosoma mansoni*. *PLoS Negl Trop Dis* 3:e504. <https://doi.org/10.1371/journal.pntd.0000504>
- Rugel AR, Guzman MA, Taylor AB, Chevalier FD, Tarpley RS, McHardy SF, Cao X, Holloway SP, Anderson TJC, Hart PJ, LoVerde PT. 2020. Why does oxamniquine kill *Schistosoma mansoni* and not *S. haematobium* and *S. japonicum*? *Int J Parasitol Drugs Drug Resist* 13:8–15. <https://doi.org/10.1016/j.ipddr.2020.04.001>
- Jewsbury JM. 1981. Metrifonate in schistosomiasis - therapy and prophylaxis. *Acta Pharmacol Toxicol (Copenh)* 49 Suppl 5:123–130. <https://doi.org/10.1111/j.1600-0773.1981.tb03263.x>
- Stohler HR. 1978. Ro 11-3128, a novel schistosomicidal compound. Proceedings of the 10th International Congress of Chemotherapy. Vol. 1, p 147–148
- Baard AP, Sommers DK, Honiball PJ, Fourie ED, du Toit LE. 1979. Preliminary results in human schistosomiasis with Ro 11-3128. *S Afr Med J* 55:617–618.
- Bennett JL. 1980. Characteristics of antischistosomal benzodiazepine binding sites in *Schistosoma mansoni*. *J Parasitol* 66:742–747.
- Park S-K, Sprague DJ, Rohr CM, Chulkov EG, Petrow I, Kumar S, Marchant JS. 2024. The anthelmintic meclonazepam activates a schistosome transient receptor potential channel. *J Biol Chem* 300:105528. <https://doi.org/10.1016/j.jbc.2023.105528>
- Gönnert R, Andrews P. 1977. Praziquantel, a new broad-spectrum antischistosomal agent. *Z F Parasitenkunde* 52:129–150. <https://doi.org/10.1007/BF00389899>
- Hunkeler W, Möhler H, Pieri L, Polc P, Bonetti EP, Cumin R, Schaffner R, Haefely W. 1981. Selective antagonists of benzodiazepines. *Nature* 290:514–516. <https://doi.org/10.1038/290514a0>
- Darragh A, Lambe R, Scully M, Brick I, O'Boyle C, Downe WW. 1981. Investigation in man of the efficacy of a benzodiazepine antagonist, Ro 15-1788. *Lancet* 2:8–10. [https://doi.org/10.1016/s0140-6736\(81\)90251-8](https://doi.org/10.1016/s0140-6736(81)90251-8)
- Roncar G, Ziegler WH, Guentert TW. 1986. Pharmacokinetics of the new benzodiazepine antagonist Ro 15-1788 in man following intravenous and oral administration. *Br J Clin Pharmacol* 22:421–428. <https://doi.org/10.1111/j.1365-2125.1986.tb02912.x>
- Coassolo P, Aubert C, Cano JP. 1985. Plasma determination of 3-methylclonazepam by capillary gas chromatography. *J Chromatogr* 338:347–355. [https://doi.org/10.1016/0378-4347\(85\)80105-5](https://doi.org/10.1016/0378-4347(85)80105-5)
- International Helminth Genomes Consortium. 2019. Comparative genomics of the major parasitic worms. *Nat Genet* 51:163–174. <https://doi.org/10.1038/s41588-018-0262-1>
- McCusker P, Mian MY, Li G, Olp MD, Tiruveedhula V, Rashid F, Golani LK, Verma RS, Smith BC, Cook JM, Chan JD. 2019. Non-sedating benzodiazepines cause paralysis and tissue damage in the parasitic blood fluke *Schistosoma mansoni*. *PLoS Negl Trop Dis* 13:e0007826. <https://doi.org/10.1371/journal.pntd.0007826>
- Johnson H, VanHooreweghe M, Satori JA, Chan JD. 2023. Schistosomes contain divergent ligand-gated ion channels with an atypical Cys-loop motif. *MicroPubl Biol* 2023. <https://doi.org/10.17912/micropub.biology.000694>
- McKernan RM, Rosahl TW, Reynolds DS, Sur C, Wafford KA, Atack JR, Farrar S, Myers J, Cook G, Ferris P, Garrett L, Bristow L, Marshall G, Macaulay A, Brown N, Howell O, Moore KW, Carling RW, Street LJ, Castro JL, Ragan CI, Dawson GR, Whiting PJ. 2000. Sedative but not anxiolytic properties of benzodiazepines are mediated by the GABA(A) receptor alpha1 subtype. *Nat Neurosci* 3:587–592. <https://doi.org/10.1038/75761>
- Pax R, Bennett JL, Fetterer R. 1978. A benzodiazepine derivative and praziquantel: effects on musculature of *Schistosoma mansoni* and *Schistosoma japonicum*. *Archives Pharmacol* 304:309–315. <https://doi.org/10.1007/BF00507974>
- Wheeler NJ, Gallo KJ, Rehborg EJG, Ryan KT, Chan JD, Zamanian M. 2022. wrmXpress: a modular package for high-throughput image analysis of parasitic and free-living worms. *PLoS Negl Trop Dis* 16:e0010937. <https://doi.org/10.1371/journal.pntd.0010937>
- Ryan KT, Wheeler NJ, Kamara IK, Johnson H, Humphries JE, Zamanian M, Chan JD. 2023. Phenotypic profiling of macrocyclic lactones on parasitic *Schistosoma* flatworms. *Antimicrob Agents Chemother* 67:e01230-22. <https://doi.org/10.1128/aac.01230-22>
- Szent A. 1977. Benzodiazepine derivatives. 4031078A. US Patent.
- Panic G, Ruf MT, Keiser J. 2017. Immunohistochemical investigations of treatment with Ro 13-3978, praziquantel, oxamniquine, and mefloquine in *Schistosoma mansoni*-infected mice. *Antimicrob Agents Chemother* 61:e01142-17. <https://doi.org/10.1128/AAC.01142-17>
- McCusker P, Rohr CM, Chan JD. 2021. *Schistosoma mansoni* alter transcription of immunomodulatory gene products following *in vivo* praziquantel exposure. *PLoS Negl Trop Dis* 15:e0009200. <https://doi.org/10.1371/journal.pntd.0009200>
- Sabah AA, Fletcher C, Webbe G, Doenhoff MJ. 1986. *Schistosoma mansoni*: chemotherapy of infections of different ages. *Exp Parasitol* 61:294–303. [https://doi.org/10.1016/0014-4894\(86\)90184-0](https://doi.org/10.1016/0014-4894(86)90184-0)
- Pham-Huy C, Villain-Pautet G, Hua H, Chikhi-Chorf N, Galons H, Thevenin M, Claude J-R, Warinet J-M. 2002. Separation of oxazepam, lorazepam, and temazepam enantiomers by HPLC on a derivatized cyclodextrin-bonded phase: application to the determination of oxazepam in plasma. *J Biochem Biophys Methods* 54:287–299. [https://doi.org/10.1016/s0165-022x\(02\)00123-9](https://doi.org/10.1016/s0165-022x(02)00123-9)
- Besnard J, Ruda GF, Setola V, Abecassis K, Rodriguez RM, Huang X-P, Norval S, Sassano MF, Shin AI, Webster LA, Simeons FRC, Stojanovski L, Prat A, Seidah NG, Constat DB, Bickerton GR, Read KD, Wetzel WC,

- Gilbert IH, Roth BL, Hopkins AL. 2012. Automated design of ligands to polypharmacological profiles. *Nature* 492:215–220. <https://doi.org/10.1038/nature11691>
33. Mahajan A, Kumar V, Mansour NRN, Bickle Q, Chibale K. 2008. Meclonazepam analogues as potential new antihelminthic agents. *Bioorg Med Chem Lett* 18:2333–2336. <https://doi.org/10.1016/j.bmcl.2008.02.077>
34. Menezes CMS, Rivera G, Alves MA, do Amaral DN, Thibaut JPB, Noël F, Barreiro EJ, Lima LM. 2012. Synthesis, biological evaluation, and structure-activity relationship of clonazepam, meclonazepam, and 1,4-benzodiazepine compounds with schistosomicidal activity. *Chem Biol Drug Des* 79:943–949. <https://doi.org/10.1111/j.1747-0285.2012.01354.x>
35. Borea PA, Gilli G. 1984. The nature of 1,4-benzodiazepines/receptor interactions. *Arzneimittelforschung* 34:649–652.
36. Braestrup C, Squires RF. 1978. Pharmacological characterization of benzodiazepine receptors in the brain. *Eur J Pharmacol* 48:263–270. [https://doi.org/10.1016/0014-2999\(78\)90085-7](https://doi.org/10.1016/0014-2999(78)90085-7)
37. Borea PA. 1983. *De novo* analysis of receptor binding affinity data of benzodiazepines. *Arzneimittelforschung* 33:1086–1088.
38. Loew GH, Nienow JR, Poulsen M. 1984. Theoretical structure-activity studies of benzodiazepine analogues. Requirements for receptor affinity and activity. *Mol Pharmacol* 26:19–34.
39. Elgarf AA, Siebert DCB, Steudle F, Draxler A, Li G, Huang S, Cook JM, Ernst M, Scholze P. 2018. Different benzodiazepines bind with distinct binding modes to GABA<sub>A</sub> receptors. *ACS Chem Biol* 13:2033–2039. <https://doi.org/10.1021/acscchembio.8b00144>
40. Masiulis S, Desai R, Uchański T, Serna Martin I, Laverty D, Karia D, Malinauskas T, Zivanov J, Pardon E, Koteka A, Steyaert J, Miller KW, Aricescu AR. 2019. GABA<sub>A</sub> receptor signalling mechanisms revealed by structural pharmacology. *Nature* 565:454–459. <https://doi.org/10.1038/s41586-018-0832-5>
41. Hansch C, Steward AR, Anderson SM, Bentley DL. 1968. Parabolic dependence of drug action upon lipophilic character as revealed by a study of hypnotics. *J Med Chem* 11:1–11. <https://doi.org/10.1021/jm00307a001>
42. Olfson M, King M, Schoenbaum M. 2015. Benzodiazepine use in the United States. *JAMA Psychiatry* 72:136–142. <https://doi.org/10.1001/jamapsychiatry.2014.1763>
43. Laconde G, Amblard M, Martinez J. 2021. Synthesis of α-amino acid *N*-carboxyanhydrides. *Org Lett* 23:6412–6416.
44. Meng EC, Goddard TD, Petersen EF, Couch GS, Pearson ZJ, Morris JH, Ferrin TE. 2023. UCSF ChimeraX: tools for structure building and analysis. *Protein Sci* 32:e4792. <https://doi.org/10.1002/pro.4792>
45. McNutt AT, Francoeur P, Aggarwal R, Masuda T, Meli R, Ragoza M, Sunseri J, Koes DR. 2021. GNINA 1.0: molecular docking with deep learning. *J Cheminform* 13:43. <https://doi.org/10.1186/s13321-021-00522-2>
46. Krivák R, Hoksza D. 2018. P2Rank: machine learning based tool for rapid and accurate prediction of ligand binding sites from protein structure. *J Cheminform* 10:39. <https://doi.org/10.1186/s13321-018-0285-8>